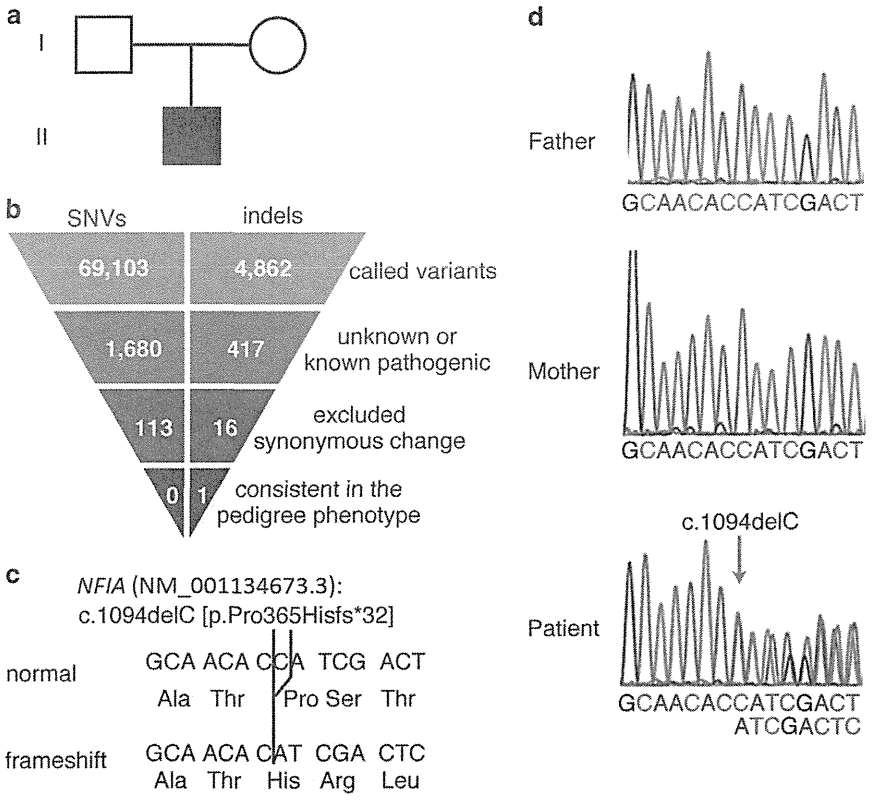

Figure 2. Genetic analysis of the pedigree. (**a**) Family tree of the pedigree. (**b**) Filtering the candidate mutations. Numbers show the patient result. The top numbers indicate number of called variants by whole-exome sequencing. The second numbers indicate number of variants after filter out known variants in databases, except for those which were also known pathogenic mutations. The third number indicates number of variants after excluded synonymous change variants. The bottom numbers indicate number of variants consistent with the phenotype in the pedigree (that is, total of the *de novo*, autosomal recessive, X-linked and compound heterozygous variants). Finally, only one deletion variant was remained. (**c**) Identified frameshift mutation in the *NFIA* gene. (**d**) Sanger sequencing of the *NFIA* mutation. Patient had a heterozygous c.1094delC mutation (arrow) not found in his parents.

the *NFIA* gene. Nine cases (6 deletions, 2 translocations and 1 intragenic deletion) of this syndrome have been reported to date,[1–7] with corpus callosum hypoplasia or defects and hydrocephalus, ventricular enlargement and developmental delays observed in all cases. Urinary tract defects, tethered spinal cord and type 1 Chiari malformation were also observed in six, four and three cases, respectively. Additionally, abnormal facies and marble skin have been reported. The present case showed ventricular enlargement, callosal agenesis, urinary tract defects, mildly dysmorphic facial features and an intelligence quotient in the borderline range. Thus, our case showed virtually the same phenotype as 1p32-p31 deletion syndrome. Since the single nucleotide deletion detected in our case is not likely to cause a position effect affecting surrounding genes, it indicates that haploinsufficiency of the *NFIA* gene is a major determinant of this syndrome.

A truncating mutation in the *NFIA* gene was previously reported in one patient with autistic spectrum disorder (c.112C>T; p.R38*),[8] but detailed clinical information was not available. Since urinary tract involvement is easily missed, it is conceivable that this previous patient may have the same phenotype, and comprehensive evaluation of the patient might uncover the underlying defects.

The *NFIA* gene encodes a member of the nuclear factor I (NFI) family of transcription factors.[9] NFI proteins control a range of key processes in central nervous system development including axon guidance and outgrowth, glial and neuronal cell differentiation, and neuronal migration.[10] Additionally, these molecules regulate midline glia formation in the cortex[11] and gliogenesis within the spinal cord.[12] Thus, NFI functional defects could result in abnormal brain formation, especially in midline structures, and spinal cord defects leading to neurogenic urinary tract dysfunction and defects. Interestingly, haploinsufficiency of the *NFIB* and *NFIX* genes, which belong to the same NFI family, also cause callosal agenesis,[13–15] and missense mutations in the *NFIX* gene cause Sotos-like syndrome.[14,16] Our case also demonstrated prominent macrocephaly, which is a major feature of Sotos syndrome. Therefore, mutations in NFI family genes may give rise to similar clinical presentations that encompass callosal agenesis and macrocephaly.

In our case, identification of the mutation by whole-exome sequencing led us to identify urinary tract defects in the presymptomatic period, and untreated higher grades of vesicoureteral reflux may have resulted in renal scar formation.[17] Therefore, whole-exome sequencing can be a powerful tool in clinical practice for early diagnosis of congenital disorders.

HGV DATABASE

The relevant data from this Data Report are hosted at the Human Genome Variation Database at http://dx.doi.org/10.6084/m9.figshare.hgv.574.

ACKNOWLEDGEMENTS

This study was supported in part by a grant for Research on Applying Health Technology from the Ministry of Health, Labour and Welfare of Japan to FM, NO, MK, MY, YK, KK and SS. We thank KA Boroevich for English proofreading.

COMPETING INTERESTS

The authors declare no conflict of interest.

REFERENCES

1 Lu W, Quintero-Rivera F, Fan Y, Alkuraya FS, Donovan DJ, Xi Q *et al.* NFIA haploinsufficiency is associated with a CNS malformation syndrome and urinary tract defects. *PLoS Genet* 2007; **3**: e80.
2 Campbell CG, Wang H, Hunter GW. Interstitial microdeletion of chromosome 1p in two siblings. *Am J Med Genet* 2002; **111**: 289–294.
3 Koehler U, Holinski-Feder E, Ertl-Wagner B, Kunz J, von Moers A, von Voss H *et al.* A novel 1p31.3p32.2 deletion involving the NFIA gene detected by array CGH in a patient with macrocephaly and hypoplasia of the corpus callosum. *Eur J Pediatr* 2010; **169**: 463–468.
4 Chen CP, Su YN, Chen YY, Chern SR, Liu YP, Wu PC *et al.* Chromosome 1p32-p31 deletion syndrome: prenatal diagnosis by array comparative genomic hybridization using uncultured amniocytes and association with NFIA haploinsufficiency, ventriculomegaly, corpus callosum hypogenesis, abnormal external genitalia, and intrauterine growth restriction. *Taiwan J Obstet Gynecol* 2011; **50**: 345–352.
5 Ji J, Salamon N, Quintero-Rivera F. Microdeletion of 1p32-p31 involving NFIA in a patient with hypoplastic corpus callosum, ventriculomegaly, seizures and urinary tract defects. *Eur J Med Genet* 2014; **57**: 267–268.
6 Shanske AL, Edelmann L, Kardon NB, Gosset P, Levy B. Detection of an interstitial deletion of 2q21-22 by high resolution comparative genomic hybridization in a child with multiple congenital anomalies and an apparent balanced translocation. *Am J Med Genet A* 2004; **131**: 29–35.
7 Rao A, O'Donnell S, Bain N, Meldrum C, Shorter D, Goel H *et al.* An intragenic deletion of the NFIA gene in a patient with a hypoplastic corpus callosum, craniofacial abnormalities and urinary tract defects. *Eur J Med Genet* 2014; **57**: 65–70.
8 Iossifov I, Ronemus M, Levy D, Wang Z, Hakker I, Rosenbaum J *et al. De novo* gene disruptions in children on the autistic spectrum. *Neuron* 2012; **74**: 285–299.
9 Qian F, Kruse U, Lichter P, Sippel AE. Chromosomal localization of the four genes (NFIA, B, C, and X) for the human transcription factor nuclear factor I by FISH. *Genomics* 1995; **28**: 66–73.
10 Mason S, Piper M, Gronostajski RM, Richards LJ. Nuclear factor one transcription factors in CNS development. *Mol Neurobiol* 2009; **39**: 10–23.
11 Shu T, Butz KG, Plachez C, Gronostajski RM, Richards LJ. Abnormal development of forebrain midline glia and commissural projections in Nfia knock-out mice. *J Neurosci* 2003; **23**: 203–212.
12 Deneen B, Ho R, Lukaszewicz A, Hochstim CJ, Gronostajski RM, Anderson DJ *et al.* The transcription factor NFIA controls the onset of gliogenesis in the developing spinal cord. *Neuron* 2006; **52**: 953–968.
13 Sajan SA, Fernandez L, Nieh SE, Rider E, Bukshpun P, Wakahiro M *et al.* Both rare and *de novo* copy number variants are prevalent in agenesis of the corpus callosum but not in cerebellar hypoplasia or polymicrogyria. *PLoS Genet* 2013; **9**: e1003823.
14 Malan V, Rajan D, Thomas S, Shaw AC, Louis Dit Picard H, Layet V *et al.* Distinct effects of allelic NFIX mutations on nonsense-mediated mRNA decay engender either a Sotos-like or a Marshall-Smith syndrome. *Am J Hum Genet* 2010; **87**: 189–198.
15 Steele-Perkins G, Plachez C, Butz KG, Yang G, Bachurski CJ, Kinsman SL *et al.* The transcription factor gene Nfib is essential for both lung maturation and brain development. *Mol Cell Biol* 2005; **25**: 685–698.
16 Yoneda Y, Saitsu H, Touyama M, Makita Y, Miyamoto A, Hamada K *et al.* Missense mutations in the DNA-binding/dimerization domain of NFIX cause Sotos-like features. *J Hum Genet* 2012; **57**: 207–211.
17 Peters CA, Skoog SJ, Arant BS Jr, Copp HL, Elder JS, Hudson RG *et al.* Summary of the AUA Guideline on Management of Primary Vesicoureteral Reflux in Children. *J Urol* 2010; **184**: 1134–1144.

Supplementary Information for this article can be found on the *Human Genome Variation* website (http://www.nature.com/hgv)

Clinical, Molecular, and Neurophysiological Features in Angelman Syndrome

Shinji Saitoh[1]

[1] Department of Pediatrics and Neonatology, Nagoya City University Graduate School of Medical Sciences, Nagoya, Japan

Address for correspondence Shinji Saitoh, MD, PhD, Kawasumi-1, Mizuho-cho, Mizuho-ku, Nagoya 467-8601, Japan (e-mail: ss11@med.nagoya-cu.ac.jp).

J Pediatr Epilepsy 2015;4:17–22.

Abstract

Angelman syndrome (AS) is a neurodevelopmental disorder associated with a unique type of epilepsy. AS is caused by loss of function of the ubiquitin protein ligase E3A (*UBE3A*) gene. Most cases of AS (70%) are caused by an approximate 5 Mb deletion in chromosome 15q11-q13 of the maternally derived allele; other causes include paternal uniparental disomy of chromosome 15 (5%), imprinting defects (5%), and *UBE3A* mutations (10%), with the genetic cause yet to be determined in the remaining 10% of cases. Many seizure types are present in AS, with myoclonic, absence, and tonic–clonic seizures being common. Characteristic findings of electroencephalography in AS include persistent rhythmic theta activity, anterior dominant rhythmic high-amplitude delta (2–3 Hz) activity or spikes and slow waves, and posterior dominant spikes and sharp waves mixed with 3 to 4 Hz high-amplitude slow waves. *UBE3A* has been shown to regulate both the glutamatergic and gamma-aminobutyric acidergic systems; further dissection of the molecular mechanisms of *UBE3A* action in mouse models and individuals with AS would facilitate a greater understanding of the pathophysiology of epilepsy.

Keywords

- Angelman syndrome
- *UBE3A*
- electroencephalography
- tonic inhibition

Introduction

Angelman syndrome (AS) is a neurodevelopmental disorder characterized by severe developmental delay, speech impairment, ataxic movement, epilepsy, and characteristic behavior, including inappropriate laughter.[1] The prevalence of AS is approximately 1 in 15,000 births, making AS one of the relatively common genetic epilepsy syndromes. Epilepsy is one of the main features of AS, and electroencephalogram (EEG) abnormalities are present in most patients. Developmental delay is usually noted at 6 months of age or later, with the average age at which infants with AS start walking independently being between 2.5 and 6 year. Loss of function of the imprinted ubiquitin protein ligase E3A (*UBE3A*) gene is responsible for most features of AS, with several genetic mechanisms underlying the loss of function of *UBE3A*.[1]

In this review, we describe the epilepsy and neurophysiological features in AS, as well as the pathophysiology underlying them.

Diagnosis of Angelman Syndrome

Consensus for Diagnostic Criteria

Consensus statements for diagnostic criteria of AS have been developed and are widely used.[2] Ninety percent of individuals with AS can be diagnosed by genetic testing, with 10% being diagnosed clinically. ►**Table 1** shows the consensus clinical features of AS. Individuals with AS do not exhibit any specific signs or symptoms during the neonatal period. Although developmental delay is noted at around 6 months of age, the characteristic clinical features fulfilling the consensus criteria appear in subsequent years. Therefore, genetic testing is helpful in making a correct diagnosis in early childhood.

received
September 8, 2014
accepted
September 17, 2014

Issue Theme Epilepsy in Numerical Chromosomal Abnormalities; Guest Editor: Toshiyuki Yamamoto, MD, PhD

DOI http://dx.doi.org/10.1055/s-0035-1554787.
ISSN 2146-457X.

Table 1 Clinical features of Angelman syndrome for diagnosis

A. Consistent (100%)
Developmental delay, functionally severe
Movement or balance disorder, usually ataxia of gait, and/or tremulous movement of limbs. Movement disorder can be mild. May not appear as frank ataxia but can be forward lurching, unsteadiness, clumsiness, or quick, jerky motions
Behavioral uniqueness: any combination of frequent laughter/smiling; apparent happy demeanor; easily excitable personality, often with uplifted hand-flapping, or waving movements; hypermotoric behavior
Speech impairment, none or minimal use of words; receptive and nonverbal communication skills higher than verbal ones
B. Frequent (more than 80%)
Delayed, disproportionate growth in head circumference, usually resulting in microcephaly (≤2 standard deviation of normal occipitofrontal circumference) by age 2 years. Microcephaly is more pronounced in those with 15q11.2-q13 deletions
Seizures, onset usually <3 years of age. Seizure severity usually decreases with age but the seizure disorder lasts throughout adulthood
Abnormal electroencephalogram, with a characteristic pattern. The electroencephalogram abnormalities can occur in the first 2 years of life and can precede clinical features, and are often not correlated to clinical seizure events
C. Associated (20–80%)
Flat occiput
Occipital groove
Protruding tongue
Tongue thrusting; suck/swallowing disorders
Feeding problems and/or truncal hypotonia during infancy
Prognathia
Wide mouth, wide-spaced teeth
Frequent drooling
Excessive chewing/mouthing behaviors
Strabismus
Hypopigmented skin, light hair, and eye color compared with family, seen only in deletion cases
Hyperactive lower extremity deep tendon reflexes
Uplifted, flexed arm position especially during ambulation
Wide-based gait with pronated or valgus-positioned ankles
Increased sensitivity to heat
Abnormal sleep–wake cycles and diminished need for sleep
Attraction to/fascination with water; fascination with crinkly items such as certain papers and plastics
Abnormal food-related behaviors
Obesity (in the older child)
Scoliosis
Constipation

Molecular Classification

Four genetic mechanisms have been identified as underlying AS (►**Fig. 1**). Appropriate genetic testing is required to identify each genetic class for a molecular diagnosis.[1]

Maternal Deletion of 15q11-q13

The most common genetic class is an approximate 5 Mb deletion on maternally derived chromosome 15, which accounts for 70% of individuals with AS. The breakpoints for the deletion reside in regions containing low copy repeat sequences and thus the size of the deletion is identical in most individuals (►**Fig. 2**). In neurons, only the maternally derived allele of *UBE3A* is expressed, while the paternally derived allele is silenced (tissue-specific imprinting). Thus, only deletions in the maternal allele result in loss of function of *UBE3A* leading to AS phenotypes. The same deletion on the paternally derived allele gives rise to the distinct Prader–Willi syndrome, which is caused by loss of function of paternally expressed genes in 15q11-q13. The deletion also encompasses several nonimprinted genes, including three genes

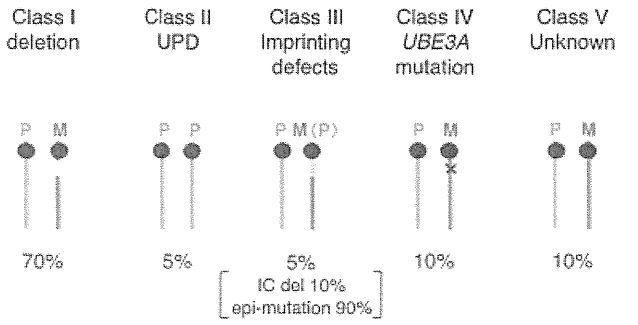

Fig. 1 Molecular classes of Angelman syndrome. The numbers at the bottom of the diagram indicate the relative frequency of each class. P, paternally derived chromosome 15; M, maternally derived chromosome 15; M(P), paternal epigenotype on maternally derived 15q11-q13; UPD, uniparental disomy; IC del, imprinting center deletion.

encoding gamma-aminobutyric acid type A ($GABA_A$) receptor subunits (►**Fig. 2**), which may modify the clinical severity of epilepsy in AS.

Paternal Uniparental Disomy of Chromosome 15

In 5% of cases, AS is due to paternal uniparental disomy (UPD) of chromosome 15 (patUPD15). Because only paternally derived alleles are present in patUPD15, functional *UBE3A* is lost, resulting in AS.

Imprinting Defects

Imprinting defects represent a unique class of genetic mechanisms responsible for AS. Imprinting defects are thought to be due to failure of the establishment and maintenance of proper imprinting of the maternally derived allele. Maternally derived 15q11-q13 fails to establish a maternal methylation pattern (epigenotype) and instead shows a paternal epigenotype; subsequently, expression of *UBE3A* is shut off, while chromosome 15 is inherited from both the mother and father. Small deletions encompassing the imprinting center (IC) are found in 10% of individuals with imprinting defects, and thus the IC is believed to be essential for the establishment of the maternal epigenotype in 15q11-q13. The remaining 90% of individuals with imprinting defects do not carry a microdeletion in IC, and this subclass is referred to as having "epi-mutations."

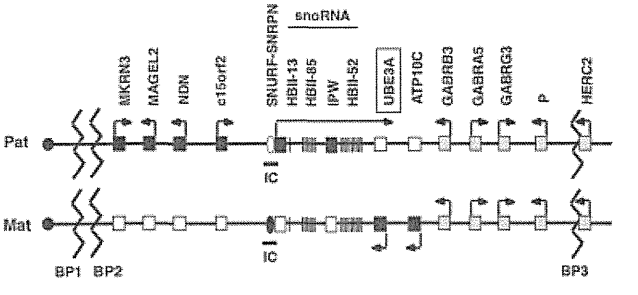

Fig. 2 Schematic map of 15q11-q13. Closed squares with arrows represent actively transcribed genes, whereas open squares represent silenced genes. Dotted squares with arrows represent biparentally expressed genes. Note ubiquitin protein ligase E3A is expressed only from the maternally derived allele, whereas *GABRB3* is expressed biparentally. IC, imprinting center; BP, breakpoint (BP1 and BP2 are proximal breakpoints and BP3 is a distal breakpoint).

UBE3A Mutations

The second most common genetic class responsible for AS accounts for 10% of cases and is due to mutations in *UBE3A*. Any mutation leading to loss of function of the maternally derived allele could be responsible for the AS phenotype; mutations of paternally derived alleles are silent. Thus, a mother of affected individuals could be a carrier of a *UBE3A* mutation.

Genetic Testing Strategies

Specific genetic tests need to be performed to determine which of the genetic mechanisms described above is responsible for AS. In the clinical setting, the following strategy is routinely used: (1) A DNA methylation test at the *SNURF-SNRPN* (small nuclear ribonucleoprotein polypeptide *N*) locus identifies maternal deletions, patUPD15, and imprinting defects, and is typically the first test recommended. (2) If the DNA methylation test is normal, the next appropriate test is for *UBE3A* mutations. (3) If the DNA methylation test is abnormal (specific for AS), a diagnosis of AS is made. However, further classification is recommended for genetic counseling. (4) If the DNA methylation test is abnormal (specific for AS), fluorescence in-situ hybridization should be performed to detect deletions. If a deletion is detected, conventional chromosome G-banding should be performed to exclude chromosomal rearrangement. (5) If the DNA methylation test is abnormal (specific for AS) and a deletion is not detected, samples from both parents should be tested for UPD (polymorphism analysis). (6) If the DNA methylation test is abnormal (specific for AS), a deletion is not detected, and patUPD15 is excluded, tests should be conducted for imprinting defects. It is also suggested that the presence of IC microdeletions be investigated.[1]

Characteristics of Epilepsy in Angelman Syndrome

Natural History

Seizures are present in most (~90%) individuals with AS, and initial seizures typically occur between 1 and 3 years of age.[3] The first seizure may be accompanied by febrile episodes. Seizure types may change depending on age, and seizure frequency often improves in late childhood.[4] However, seizures continue into adulthood and may even increase.

Seizure Manifestation

Many seizure types, both generalized and focal, are present in individuals with AS.[3] Myoclonic, myoclonic absences, atypical absences, atonic, and tonic–clonic seizures are the most common seizure types, indicating that generalized seizures are common. Infantile spasms are rarely associated with AS.

Nonconvulsive status epilepticus is well recognized in AS, usually in childhood. It is not easy to determine whether nonconvulsive status epilepticus is generalized or complex

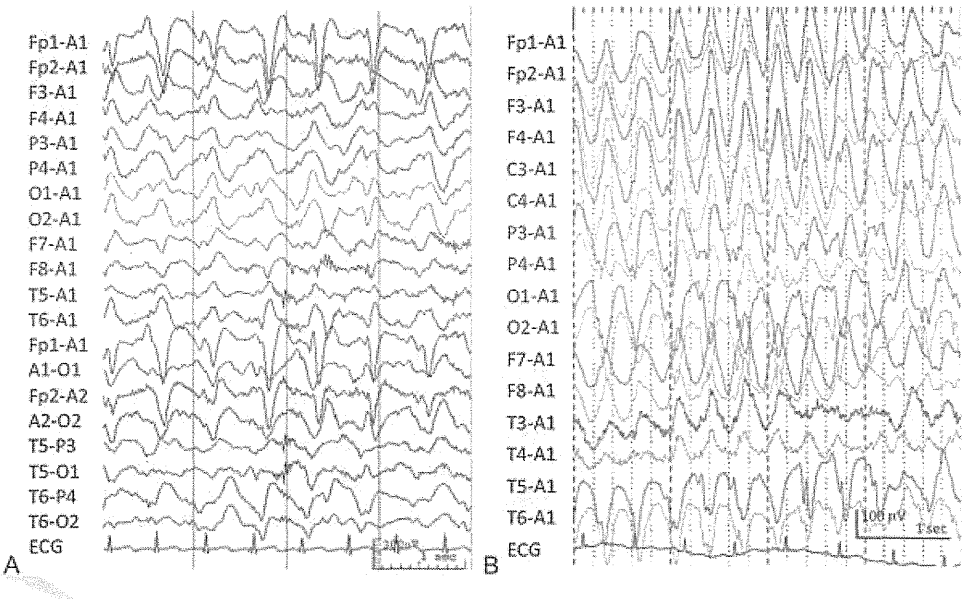

Fig. 3 Representative electroencephalograms. (A) Anterior dominant triphasic sharp waves. (B) Posterior dominant high-voltage slow waves with spike components.

partial status. Sometimes, absences with myoclonic status may occur.

Tremor or tremulous movements may occur and disturb daily life if severe. Such prolonged tremulous movements often emerge in adolescents or adults. Although not conclusive, these tremors have been attributed to cortical myoclonus.[5,6]

Electroencephalogram Characteristics

Evolution of Electroencephalogram

EEG abnormalities in patients with AS were originally reported by Boyd et al[7] and later confirmed by others.[8,9] Three EEG patterns are known to be associated with AS, as detailed below. (1) Persistent rhythmic theta activity. Approximately 4 to 6 Hz, 200 μV or higher amplitude activity is predominantly present and often generalized in awake recordings. This theta activity tends to persist during eye closure, which is characteristic of AS. This pattern tends to disappear after 12 years of age. (2) Rhythmic high-amplitude delta (2–3 Hz) activity or spikes and slow waves predominantly appear in the anterior regions (►**Fig. 3A**). Slow wave activity tends to be generalized. A variation of this pattern includes rhythmic triphasic high-amplitude (200–500 μV) 2 to 3 Hz activity in the frontal regions. This pattern has been reported to be present before the clinical diagnosis of AS.[3] (3) Spikes and sharp waves mixed with 3 to 4 Hz high-amplitude slow waves in the posterior regions, often facilitated by eye closure (►**Fig. 3B**). EEG abnormalities in the posterior regions have been reported to be the most frequent findings in young children.[8]

Abnormal EEG patterns appear in infancy before the onset of seizures, providing an important diagnostic clue. In younger patients, EEG patterns are more prominent and may appear as hypsarrhythmia in infancy. The amplitude of slow wave discharges gradually decreases with age. In adults, high-amplitude slow wave discharges tend to disappear, and epileptic discharges decrease. However, intermittent rhythmic slow waves mixed with spikes or sharp waves in the frontal regions tend to persist in adults. It should be noted that some individuals with AS do not show typical EEG abnormalities, and that a lack of a characteristic EEG pattern does not exclude a diagnosis of AS.[8]

Other Neurophysiological Findings

Several neurophysiological studies have indicated that tremulous movements, or myoclonus, are of cortical origin. For example, Guerrini et al[5] reported that rhythmic myoclonus in AS is accompanied by short bursts of rhythmic 5 to 10 Hz EEG activity. Goto et al[6] performed jerk-locked averaging and demonstrated cortical activity preceding the electromyogram, suggesting a cortical origin of the tremulous movements.

Egawa et al[10] performed magnetoencephalography on individuals with AS and revealed aberrant somatosensory-evoked responses only in those subjects with a deletion in 15q11-q13; AS individuals without a deletion in 15q11-q13 did not exhibit any abnormalities. Furthermore, the abnormal somatosensory-evoked responses were improved when benzodiazepines, which enhance GABA receptor function, were administrated to the subjects. Because three $GABA_A$ receptor subunit genes are also deleted in AS patients with the 15q11-q13 deletion, Egawa et al[10] hypothesized that heterozygous deletion of $GABA_A$ receptor subunit genes contributes to the pathophysiology of AS through GABAergic dysfunction.

Genotype–Phenotype Correlation

Individuals with AS who have the common deletion exhibit typical and the most severe phenotypes, whereas those without a deletion (UPD and imprinting defect) exhibit

relatively less severe phenotypes, less severe seizures, and milder abnormalities on EEG.[11–13] In addition, individuals with *UBE3A* mutations exhibit less severe phenotypes than those with a deletion, but the clinical severity of AS varies depending on the nature of the mutation.[11,13]

Pathophysiology of Epilepsy in Angelman Syndrome

Function of *UBE3A*

Loss of function of *UBE3A* is the major determinant of AS phenotypes. *UBE3A* is located in the imprinted domain of 15q11-q13 and is expressed only from the maternally derived allele. Imprinted expression of *UBE3A* is restricted in the brain and both alleles (maternal and paternal) are active in other tissues, explaining why the clinical features of AS are restricted to neurological features.[14]

UBE3A, alternatively known as E6-associated protein, is a ubiquitin E3 ligase that recognizes certain target proteins and ubiquitinates them. Ubiquitinated proteins are delivered to the proteasome and degraded there. Loss of function of a ubiquitin protein ligase leads to accumulation of undegraded target proteins. Therefore, identification of UBE3A target proteins is crucial to understanding the role of UBE3A in the brain. Two such candidate proteins have been identified.

Arc was the first protein shown to be a target of UBE3A in the brain. Greer et al[15] found that Arc is a target of UBE3A and that accumulation of Arc in Ube3a-knockout mice subsequently led to decrease in the number of α-amino-3-hydroxy-5-methyl-4-isoxazole propionic acid (AMPA) receptors at glutamatergic excitatory synapses. Because AMPA receptors play a fundamental role in experience-dependent synapse plasticity, Greer et al[15] concluded that deregulation of AMPA receptor expression at synapses may contribute to the cognitive dysfunction in AS. However, it is not definitively known whether this deregulation also contributes to epilepsy.

The second protein identified as a target of UBE3A was GABA transporter 1 (GAT1), which is a GABA transporter. Egawa et al[16] demonstrated that GAT1 is a target of UBE3A in the brain. Lack of UBE3A induced overexpression of GAT1, which subsequently decreased extrasynaptic concentrations of GABA, resulting in decreased tonic inhibition in cerebellar granular cells in mice. Decreased tonic inhibition may underlie motor dysfunction in AS. However, it is conceivable that aberrant tonic inhibition may be present outside the cerebellum and contribute to cognitive dysfunction or epilepsy. In humans, a magnetoencephalographic study by Egawa et al[10] suggested involvement of the GABAergic system in patients with AS, and this was supported by the findings of the positron emission tomography of Asahina et al.[17]

Involvement of GABAergic System

Tonic inhibition is mainly seen in the cerebellum, but it is conceivable that aberrant tonic inhibition may be present outside the cerebellum. Indeed, dysfunction of tonic inhibition has been reported to be associated with autism; thus, aberrant tonic inhibition may contribute to cognitive dysfunction or epilepsy in AS.[18]

GABRB3, which encodes a subunit of $GABA_A$ receptors, resides in the common deletion of AS. *GABRB3* is predominantly expressed in the fetal brain and adult hippocampus, and is a potential candidate to modulate the severity of epilepsy in individuals with AS. This idea is supported by the fact that individuals with AS who have the common deletion exhibit more severe clinical and neurophysiological features, including epilepsy, than those without the common deletion.[10] In mice, heterozygous and homozygous deletion of *GABRB3* has been reported to cause epilepsy.[19] In addition, heterozygous mutations in *GABRB3* have been identified in patients with childhood absence epilepsy.[20] Furthermore, *UBE3A* has been hypothesized to modulate *GABRB3* expression.[21] Therefore, dysfunction of the GABAergic system appears to be an important contributor to epilepsy in AS.

Management

Most patients need to be treated with antiepileptic drugs to control seizures. However, there are no evidence-based studies of the use of antiepileptic drugs in AS, and the use of these drugs is based primarily on the experience of experts. Sodium valproate (VPA) is the most commonly used antiepileptic drug, followed by clonazepam (CZP).[3] In most patients, seizures can be controlled by VPA only or VPA plus CZP, but in some patients the seizures may be difficult to control, especially in childhood. Seizure control tends to be easier in adults.

Other benzodiazepines, such as clobazam, appear to be as effective as CZP in controlling seizures.[3] Ethosuximide has also been reported to be effective.[22] New types of antiepileptic drugs, including topiramate, lamotrigine, and levetiracetam, appear to be good alternatives, but information about these drugs is limited.[23–25]

Some antiepileptic drugs that may exacerbate generalized seizures can aggravate seizures in AS, for example, carbamazepine. It is recommended that these types of antiepileptic drugs be avoided, particularly for the treatment of nonconvulsive status epilepticus.[3]

In conclusion, individuals with AS exhibit distinct epileptic features and neurophysiological findings. From a clinical viewpoint, understanding the characteristic findings of AS will help identify individuals suspected of having AS early in the clinical course, leading to proper genetic testing. From the viewpoint of basic science, AS is an invaluable model for understanding the complex pathophysiology underlying epilepsy, intellectual disability, and autism.

References

1 Williams CA, Driscoll DJ, Dagli AI. Clinical and genetic aspects of Angelman syndrome. Genet Med 2010;12(7):385–395
2 Williams CA, Beaudet AL, Clayton-Smith J, et al. Angelman syndrome 2005: updated consensus for diagnostic criteria. Am J Med Genet A 2006;140(5):413–418

3 Pelc K, Boyd SG, Cheron G, Dan B. Epilepsy in Angelman syndrome. Seizure 2008;17(3):211–217
4 Uemura N, Matsumoto A, Nakamura M, et al. Evolution of seizures and electroencephalographical findings in 23 cases of deletion type Angelman syndrome. Brain Dev 2005;27(5):383–388
5 Guerrini R, De Lorey TM, Bonanni P, et al. Cortical myoclonus in Angelman syndrome. Ann Neurol 1996;40(1):39–48
6 Goto M, Saito Y, Honda R, et al. Episodic tremors representing cortical myoclonus are characteristic in Angelman syndrome due to UBE3A mutations. Brain Dev 2015;37(2):216–222
7 Boyd SG, Harden A, Patton MA. The EEG in early diagnosis of the Angelman (happy puppet) syndrome. Eur J Pediatr 1988;147(5): 508–513
8 Laan LA, Vein AA. Angelman syndrome: is there a characteristic EEG? Brain Dev 2005;27(2):80–87
9 Leyser M, Penna PS, de Almeida AC, Vasconcelos MM, Nascimento OJ. Revisiting epilepsy and the electroencephalogram patterns in Angelman syndrome. Neurol Sci 2014;35(5):701–705
10 Egawa K, Asahina N, Shiraishi H, et al. Aberrant somatosensory-evoked responses imply GABAergic dysfunction in Angelman syndrome. Neuroimage 2008;39(2):593–599
11 Lossie AC, Whitney MM, Amidon D, et al. Distinct phenotypes distinguish the molecular classes of Angelman syndrome. J Med Genet 2001;38(12):834–845
12 Saitoh S, Wada T, Okajima M, Takano K, Sudo A, Niikawa N. Uniparental disomy and imprinting defects in Japanese patients with Angelman syndrome. Brain Dev 2005;27(5):389–391
13 Minassian BA, DeLorey TM, Olsen RW, et al. Angelman syndrome: correlations between epilepsy phenotypes and genotypes. Ann Neurol 1998;43(4):485–493
14 Yamasaki K, Joh K, Ohta T, et al. Neurons but not glial cells show reciprocal imprinting of sense and antisense transcripts of Ube3a. Hum Mol Genet 2003;12(8):837–847
15 Greer PL, Hanayama R, Bloodgood BL, et al. The Angelman Syndrome protein Ube3A regulates synapse development by ubiquitinating arc. Cell 2010;140(5):704–716
16 Egawa K, Kitagawa K, Inoue K, et al. Decreased tonic inhibition in cerebellar granule cells causes motor dysfunction in a mouse model of Angelman syndrome. Sci Transl Med 2012;4(163):163ra157
17 Asahina N, Shiga T, Egawa K, Shiraishi H, Kohsaka S, Saitoh S. [(11) C]flumazenil positron emission tomography analyses of brain gamma-aminobutyric acid type A receptors in Angelman syndrome. J Pediatr 2008;152(4):546–549, 549.e1–549.e3
18 Egawa K, Fukuda A. Pathophysiological power of improper tonic GABA(A) conductances in mature and immature models. Front Neural Circuits 2013;7:170
19 DeLorey TM, Handforth A, Anagnostaras SG, et al. Mice lacking the beta3 subunit of the GABAA receptor have the epilepsy phenotype and many of the behavioral characteristics of Angelman syndrome. J Neurosci 1998;18(20):8505–8514
20 Tanaka M, Olsen RW, Medina MT, et al. Hyperglycosylation and reduced GABA currents of mutated GABRB3 polypeptide in remitting childhood absence epilepsy. Am J Hum Genet 2008;82(6): 1249–1261
21 Tanaka M, DeLorey TM, Delgado-Escueta A, Olsen RW. GABRB3, epilepsy, and neurodevelopment. In: Noebels JL, Avoli M, Rogawski MA, Olsen RW, Delgado-Escueta AV, eds. Jasper's Basic Mechanisms of the Epilepsies. 4th ed. Bethesda, MD: National Center for Biotechnology Information (US); 2012:1–15
22 Sugiura C, Ogura K, Ueno M, Toyoshima M, Oka A. High-dose ethosuximide for epilepsy in Angelman syndrome: implication of GABA(A) receptor subunit. Neurology 2001;57(8):1518–1519
23 Franz DN, Glauser TA, Tudor C, Williams S. Topiramate therapy of epilepsy associated with Angelman's syndrome. Neurology 2000; 54(5):1185–1188
24 Dion MH, Novotny EJ Jr, Carmant L, Cossette P, Nguyen DK. Lamotrigine therapy of epilepsy with Angelman's syndrome. Epilepsia 2007;48(3):593–596
25 Weber P. Levetiracetam in nonconvulsive status epilepticus in a child with Angelman syndrome. J Child Neurol 2010;25(3): 393–396

Editorial

Ciliopathy in PCS (MVA) syndrome

Tatsuo Miyamoto and Shinya Matsuura

The spindle assembly checkpoint (SAC) is a surveillance mechanism of faithful chromosome segregation during mitosis. Budding uninhibited by benzimidazole-related-1 (BubR1) plays a central role in the SAC through inhibition of anaphase promoting complex/cyclosome (APC/C) activity until all chromosomes have established proper attachment to the mitotic spindle. Loss-of-function mutations in the *BUB1B* gene, encoding BubR1, cause a rare autosomal recessive disorder: premature chromatid separation (PCS) syndrome (Mendelian Inheritance in Man [MIM] 176430), which is also known as mosaic variegated aneuploidy (MVA) syndrome (MIM 257300) [1]. PCS (MVA) syndrome can also be caused by an intergenic mutation 44-kb upstream of the *BUB1B* gene, which suppresses the transcription level of *BUB1B* [2]. PCS (MVA) syndrome is cytogenetically characterized by PCS in > 50% of metaphase cells as well as the presence of mosaic aneuploidy [2]. Patients with the syndrome show an increased genetic predisposition to Wilms tumor and rhabdomyosarcoma, which may be attributed to the loss of SAC function. Patients also present with cataracts, uncontrollable chronic seizures, Dandy-Walker complex, polycystic kidneys and obesity. These clinical symptoms imply an additional function of BubR1 other than SAC in the context of morphogenesis.

The primary cilium is a hair-like, microtubule-based, nonmotile organelle formed on the surface of quiescent mammalian cells. It receives extracellular information and transmits signals required for cell proliferation, tissue development, and tissue homeostasis. Ciliary dysfunction is causally linked to the group of human disorders known as ciliopathies, which include Bardet-Biedl syndrome, nephronophthisis, Meckel-Gruber syndrome, Joubert syndrome, and Oral-facial-digit syndrome. To date, more than 50 loci associated with ciliopathy have been reported. In addition to these, Baker and Beales proposed that at least 193 diseases in the Online Mendelian Inheritance in Men database (OMIM, www.ncbi.nlm.nih.gov/sites/entrez?db = OMIM) can potentially be categorized as ciliopathies [3]. Patients with a ciliopathy show a series of clinical features including polycystic kidneys, polydactyly, obesity, situs inversus, and neuronal and other developmental abnormalities. Overlap of the clinical spectrum of PCS (MVA) syndrome with those of the ciliopathies has led us to explore whether BubR1 is required for primary cilium formation. We found that skin fibroblasts from PCS (MVA) patients exhibit impaired ciliogenesis, thus PCS (MVA) syndrome is a ciliopathy [4]. Interestingly, *BubR1*-knockdown medaka fish also showed ciliopathy-like phenotypes, such as defective cerebellar development and disrupted left-right asymmetry of the embryo. These results indicated that the role of BubR1 in primary cilium formation is conserved among vertebrates [4]. However, little is known about the molecular basis underlying defective ciliogenesis in PCS (MVA) syndrome.

Primary cilium formation and disassembly are tightly regulated in a cell cycle-dependent manner. In the quiescent G0 phase, centrosomes are anchored to the apical plasma membrane, and primary cilia assemble from the basal bodies transformed from the mother centrioles of the centrosome. When quiescent G0 phase cells re-enter the cell cycle, primary cilium disassembly occurs, suppressing inappropriate ciliogenesis during the proliferative phase. This negative regulation of primary cilium formation is required for the release of centrioles from the apical membrane to form a mitotic bipolar spindle in the context of cell proliferation. Recent studies have revealed that a mitotic kinase, polo-like kinase-1 (PLK1), activates a tubulin deacetylase, HDAC6, to destabilize the axonemal microtubules and initiate primary cilium disassembly following growth stimulation [5]. PLK1 phosphorylates various substrates to control mitotic spindle assembly and chromosome segregation, however the molecular mechanism of PLK1-mediated primary cilium disassembly is not well understood. Importantly, it was reported that KIF24, which belongs to the kinesin-13 family along with KIF2A, KIF2B and MCAK/KIF2C, depolymerizes centriolar microtubules to suppress inappropriate ciliogenesis during the proliferative phase [6]. Kinesin-13 proteins do not move along microtubules for intracellular transport but have microtubule depolymerizing activity. PLK1 phosphorylates KIF2A, KIF2B and MCAK/KIF2C to enhance microtubule depolymerizing activity for mitotic progression. Recently, we demonstrated that PLK1 phosphorylates KIF2A at T554 at the mother centriole, to promote its microtubule depolymerizing activity and drive primary cilium disassembly in a growth signal-dependent manner [7]. Together, we concluded that the PLK1-KIF2A axis is defined as a ciliary disassembly pathway coupled with cell proliferation.

We previously found that BubR1 localizes to centrosomes during interphase to inhibit premature activation of PLK1, and that PCS (MVA) syndrome patient

cells show constitutive activation of PLK1 throughout the cell cycle. Inhibition of *PLK1* and *KIF2A* in patient cells restores ciliogenesis [7], indicating that aberrant activation of the PLK1-KIF2A axis contributes to the ciliopathy-associated features in PCS (MVA) syndrome. PLK1 and KIF2A are up-regulated in many types of cancer cells. Further studies on the PLK1-KIF2A pathway in primary cilium disassembly will explore therapeutic opportunities against not only the ciliopathies but also various cancers.

Shinya Matsuura: Department of Genetics and Cell Biology, Research Institute for Radiation Biology and Medicine, Hiroshima University, Hiroshima, Japan

Correspondence to: *Shinya Matsuura,* ***email*** *shinya@hiroshima-u.ac.jp*

Keywords: primary cilium, ciliopathy, spindle assembly checkpoint, mitotic kinase, mitotic kinesin

Received: July 24, 2015

Published:

REFERENCES

1. Hanks S, et al. Nature Genet. 2004; 36: 1159-1161
2. Ochiai H, et al. Proc. Natl. Acad. Sci. U S A. 2014; 111: 1461-1466.
3. Baker K and Beales PL. Am J Med Genet Part C. 2009; 151C: 281-295.
4. Miyamoto, T et al. Hum Mol Genet. 2011; 20: 2058-2070
5. Lee KH, et al. EMBO J. 2012; 31: 3104-3117.
6. Kobayashi T, et al. Cell. 2011; 145: 914-925.
7. Miyamoto T, et al. Cell Rep. 2015; S2211-1247(15)00004-2.

CLINICAL GENETICS An International Journal of Genetics, Molecular and Personalized Medicine

Clin Genet 2015: 88: 261–266
Printed in Singapore. All rights reserved

CLINICAL GENETICS
doi: 10.1111/cge.12496

Short Report

Autosomal recessive cystinuria caused by genome-wide paternal uniparental isodisomy in a patient with Beckwith–Wiedemann syndrome

Ohtsuka Y, Higashimoto K, Sasaki K, Jozaki K, Yoshinaga H, Okamoto N, Takama Y, Kubota A, Nakayama M, Yatsuki H, Nishioka K, Joh K, Mukai T, Yoshiura K-i, Soejima H. Autosomal recessive cystinuria caused by genome-wide paternal uniparental isodisomy in a patient with Beckwith–Wiedemann syndrome.
Clin Genet 2015: 88: 261–266. © John Wiley & Sons A/S. Published by John Wiley & Sons Ltd, 2014

Approximately 20% of Beckwith–Wiedemann syndrome (BWS) cases are caused by mosaic paternal uniparental disomy of chromosome 11 (pUPD11). Although pUPD11 is usually limited to the short arm of chromosome 11, a small minority of BWS cases show genome-wide mosaic pUPD (GWpUPD). These patients show variable clinical features depending on mosaic ratio, imprinting status of other chromosomes, and paternally inherited recessive mutations. To date, there have been no reports of a mosaic GWpUPD patient with an autosomal recessive disease caused by a paternally inherited recessive mutation. Here, we describe a patient concurrently showing the clinical features of BWS and autosomal recessive cystinuria. Genetic analyses revealed that the patient has mosaic GWpUPD and an inherited paternal homozygous mutation in *SLC7A9*. This is the first report indicating that a paternally inherited recessive mutation can cause an autosomal recessive disease in cases of GWpUPD mosaicism. Investigation into recessive mutations and the dysregulation of imprinting domains is critical in understanding precise clinical conditions of patients with mosaic GWpUPD.

Conflict of interest

The authors have no competing financial interests to declare.

Y. Ohtsuka[a], K. Higashimoto[a], K. Sasaki[b], K. Jozaki[a], H. Yoshinaga[a], N. Okamoto[c], Y. Takama[d], A. Kubota[d], M. Nakayama[e], H. Yatsuki[a], K. Nishioka[a], K. Joh[a], T. Mukai[f], K.-i. Yoshiura[b] and H. Soejima[a]

[a]Division of Molecular Genetics and Epigenetics, Department of Biomolecular Sciences, Faculty of Medicine, Saga University, Saga, Japan, [b]Department of Human Genetics, Nagasaki University Graduate School of Biomedical Sciences, Nagasaki, Japan, [c]Department of Medical Genetics , [d]Department of Pediatric Surgery , [e]Department of Pathology, Osaka Medical Center and Research Institute for Maternal and Child Health, Osaka, Japan, and [f]Nishikyushu University, Saga, Japan

Key words: Beckwith–Wiedemann syndrome – cystinuria – genome-wide paternal uniparental disomy mosaicism – *SLC3A1* – *SLC7A9*

Corresponding author: Hidenobu Soejima, Division of Molecular Genetics and Epigenetics, Department of Biomolecular Sciences, Faculty of Medicine, Saga University, 5-1-1 Nabeshima, Saga 849-8501, Japan.
Tel.: +81 952 34 2260;
fax: +81 952 34 2067;
e-mail: soejimah@med.saga-u.ac.jp

Received 8 July 2014, revised and accepted for publication 27 August 2014

Beckwith–Wiedemann syndrome (BWS) (OMIM #130650) is an imprinting disorder characterized by peculiar prenatal and postnatal macrosomia, macroglossia, and abdominal wall defects. There are various genetic and epigenetic abnormalities that can cause BWS, although paternal uniparental disomy of 11p15 (pUPD11) accounts for around 20% of cases (1, 2). The minimum pUPD size is approximately 2.7 Mb from

the telomere of 11p, including both imprinting control regions, *H19*DMR and *Kv*DMR1 (3). pUPD11 causes hypermethylation of *H19*DMR and hypomethylation of *Kv*DMR1, which leads to overexpression of *IGF2* and reduced expression of *H19* and *CDKN1C*. In its most wide-reaching variety, pUPD acts on the whole genome, and is denoted as genome-wide pUPD (GWpUPD). Non-mosaic GWpUPD results in the formation of a hydatidiform mole, while individuals with GWpUPD mosaicism are born alive (2). GWpUPD patients usually show clinical features of BWS and other variable features thought to depend on the mosaic ratio, the imprinting status of other chromosomes such as chromosomes 6, 14, 15, and 20 (pUPDs of these chromosomes cause other imprinting disorders), and paternally inherited recessive mutations (4). However, to date, there have been no reports of a mosaic GWpUPD patient with an autosomal recessive disease caused by a paternally inherited recessive mutation.

Cystinuria (OMIM #220100) is an autosomal recessive disorder characterized by impaired epithelial cell transport of cystine and dibasic amino acids (lysine, ornithine, and arginine) in the proximal renal tubule and gastrointestinal tract. The impaired renal reabsorption and the low solubility of cystine cause the formation of calculi in the urinary tract (5). Causative genes for cystinuria include *SLC3A1* and *SLC7A9*. These genes encode proteins that comprise the rBAT/$b^{0,+}$AT heterodimer, which mediates the exchange of extracellular cationic amino acids and cystine for intracellular neutral amino acids (6).

We investigated a patient with clinical features of both BWS and cystinuria. Genetic analyses revealed that the patient harbored mosaic GWpUPD and inherited a homozygous mutation of *SLC7A9* paternally. This is the first reported case of a patient with these features exhibited concurrently.

Materials and methods

Patient report

The female infant with a karyotype of 46,XX was the first-born baby to non-consanguineous, healthy, Japanese parents after 34 weeks and 6 days of gestation. Her birth weight was 4254 g [+6.8 SD (standard deviation)], and she exhibited omphalocele, macroglossia, and nevus flammeus on her forehead. These conditions satisfy the diagnostic criteria for BWS as described by Weksberg et al. (7). After birth, she also manifested persistent hyperinsulinemic hypoglycemia and an extremely high level of serum alpha-fetoprotein (300,000 ng/ml). She was diagnosed with diffuse nesidioblastosis in the pancreatic body, and a partial pancreatectomy was performed twice, at 2 months and at 8 years of age (8). In addition, at puberty she had bilateral breast fibroadenomas and an ovarian adenofibroma, as recently reported (9). She did not develop any mental or motor delay.

Atrophy of the left kidney and enlargement of the right kidney were detected at birth, and urinary stones in the bladder and medullary calcinosis in both kidneys were detected at 10 months of age (Fig. 1). The

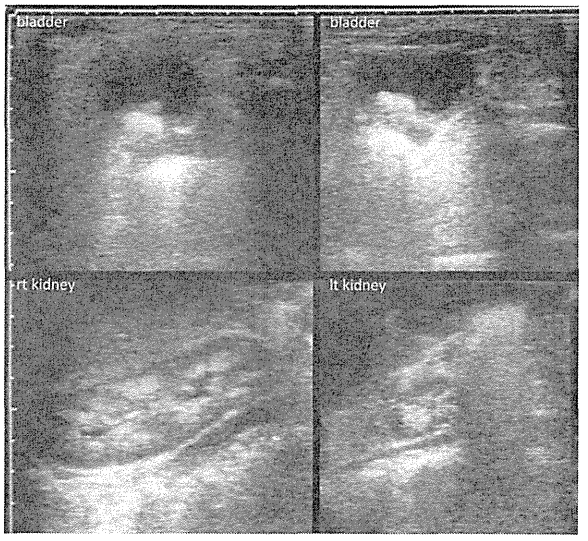

Fig. 1. Sonography of urolithiasis. Ultrasound images of the patient at one year of age shows a 1 cm stone in the bladder and medullary calcinosis in both kidneys. Atrophy of the left kidney was diagnosed at birth.

urinary amino acid analysis revealed high concentrations of cystine (551 μmol/l), lysine (5175 μmol/l), and arginine (3837 μmol/l), and cystine crystals were visible in a urine sample. Therefore, she was also diagnosed with cystinuria. Her parents had no history of urolithiasis; however, cystine and lysine in the father's urine were moderately elevated (296 μmol/l and 850 μmol/l, respectively).

This study was approved by the Ethics Committee for Human Genome and Gene Analyses of the Faculty of Medicine, Saga University.

DNA isolation

Genomic DNA was extracted from the peripheral blood of the patient and her parents, the patient's pancreas, and urine using commercially available DNA extraction kits.

SNP array analysis

Single nucleotide polymorphism (SNP) array analysis was performed with Genome-Wide Human SNP Array 5.0 (Affymetrix, Santa Clara, CA) according to the manufacturer's protocol. The genotype was analyzed using GENOTYPING CONSOLE (GTC) 4.1 software (Affymetrix). Copy number, allele ratio, and trio SNP analyses were performed using PARTEK GENOMICS SUITE version 6.6 beta (Partek Inc., St. Louis, MO). A reference generated from 89 Japanese samples was used. The genomic positions of the SNPs corresponded to GRCh37/hg19.

Mutation analyses of *SLC3A1* and *SLC7A9* genes

All coding exons and flanking intronic regions of *SLC3A1* and *SLC7A9* genes were amplified by polymerase chain reaction (PCR) and directly sequenced.

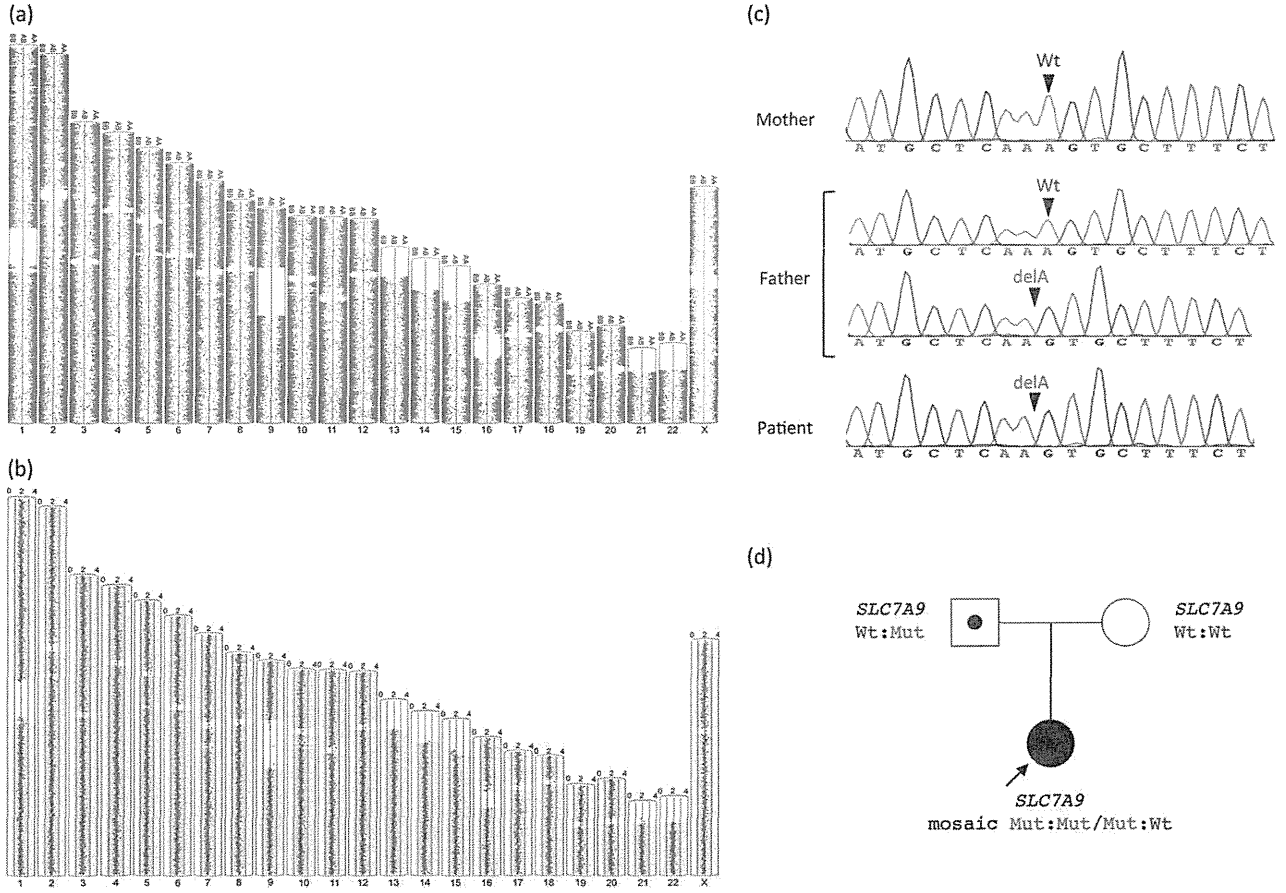

Fig. 2. Results of single nucleotide polymorphism (SNP) array analysis and mutation analysis of a cystinuria causative gene, *SLC7A9*. (**a**, **b**) Results of patient SNP array analysis. Genotyping (**a**) showed homozygous (AA or BB) results for almost all SNPs throughout all chromosomes, and absence of aberrant copy number variation (**b**); this evidence supports the notion of mosaicism for genome-wide paternal uniparental disomy (GWpUPD) of isodisomic androgenetic cells and normal biparental cells. (**c**) Results of mutation analysis of a cystinuria causative gene, *SLC7A9*. Sanger sequencing revealed a single-base deletion in exon 10 in both the father and the patient. Polymerase chain reaction (PCR)-cloning-sequencing revealed four wild-type clones and nine mutant clones in the father, indicating heterozygosity for the mutation. PCR direct sequencing showed that the patient seemed to be homozygous for the mutation because of a high mosaic ratio for GWpUPD. The mother did not have the mutation. (**d**) Patient's family pedigree. The *SLC7A9* mutation found in the patient was paternally inherited. In the patient, cells with GWpUPD were homozygous for the mutation, whereas biparental cells were heterozygous, containing both the mutation and the maternally inherited wild-type allele.

The PCR product of *SLC7A9* exon 10 in the father was cloned into a pT7Blue T-Vector (Novagen, San Diego, CA), and individual clones were sequenced. Primers for the mutation analyses are listed in Table S1, Supporting Information.

Results

To identify the potential cause of the BWS, we first performed methylation-sensitive Southern blots of two imprinting control regions at 11p15, *H19*DMR, and *Kv*DMR1. The methylation index (MI) was 99% at *H19*DMR and 2% at *Kv*DMR1 (Fig. S1). Because *H19*DMR is methylated on the paternal allele and *Kv*DMR1 is methylated on the maternal allele, pUPD of the region with a high mosaic ratio was strongly suggested.

We then performed microarray analysis of the patient, father, and mother SNP trios using SNP Array 5.0. The results showed two normal copies in the patient and her parents; however, the patient's genotype contained homozygous (AA or BB) results for almost all SNPs throughout all chromosomes (Fig. 2a,b). The genotyping of the trios indicated that the informative SNPs in the patient had been transmitted via paternal uniparental inheritance (data of chromosomes 2 and 19 are shown in Fig. S2). To calculate the mosaic ratio, we quantitatively analyzed microsatellite markers across all chromosomes except chromosome Y. In the patient, the average mosaic ratio of all informative markers was 91% in the peripheral blood and 83% in the pancreas (Table S2). These results indicated GWpUPD mosaicism of isodisomic androgenetic cells and normal biparental cells. Because mosaic GWpUPD necessarily includes 11p15.4-p15.5, we concluded that the causative abnormality for the BWS phenotype was pUPD11.

Finally, because the patient was diagnosed with autosomal recessive cystinuria, we performed mutation analyses of the supposed causative genes for cystinuria, *SLC3A1* at 2p21 and *SLC7A9* at 19q13.1. The

Table 1. Literature review of live-born patients with genome-wide paternal UPD[a]

	Our patient	Johnson et al. (13)	Kalish et al. (12)			Gogiel et al. (15)	Inbar-Feigenberg et al. (14)	Yamazawa et al. (4)	Romanelli et al. (16)	Wilson et al. (17)		Reed et al. (18)	Giurgea et al. (19)	Bryke and Garber (20)	Hoban et al. (21)
			Patient #1	Patient #2	Patient #3					Patient #1	Patient #2				
Gestational age	34 weeks 6 days	30 weeks 6 days	31 weeks 5 days	30 weeks 6 days	24 weeks 1 days	37 weeks	33 weeks	34 weeks		36 weeks	29 weeks 6 days	30 weeks 4 days	35 weeks		42 weeks
Birth weight (g)	4254	2460				3850	2270	3730	3750			1110	2260		
Weight percentile	>97th	>97th	85th	95th	50th	>90th	75th	>97th		>97th	>90th		25–50th		
Macroglossia	+			+		+		+		+					
Abdominal wall defect	+	+	+	+	+	+	+	+		+	+				
Visceromegaly	+		+	+	+	+	+	+		+	+			+	
Hemihyperplasia		+	+	+		+	+	+	+		+		+	+	+
Hypoglycemia	+	+	+	+	+	+	+	+	+	+	+		+		
Cutaneous abnormality	+		+	+			+		+		+			+	
Cardiac abnormality	+		+			+	+			+				+	
Neurological abnormality			+				+	+	+	+	+			+	
Tumor development	+		+	+	+	+	+	+	+	+	+	+	+	+	+
Failure to thrive				+				+		+	+			+	
Placental abnormality	+		+	+		+	+	+			+	+			
Other abnormality			+	+	+	+	+	+	+	+	+			+	
Features estimated paternal UPD	UPD11	UPD11	UPD11, 14	UPD11	UPD11	UPD11, 14	UPD11, 15, 20	UPD11, 14, 15	UPD11, 15	UPD11	UPD11		UPD11	UPD6, 14, 15, 20	UPD11
Other findings	Cystinuria (homozygous mutation of *SLC7A9*)	Hyperkalemia, abdominal swelling, deceased		Peripheral pulmonic stenosis, small bowel obstructions	Respiratory distress, cliteromegaly, deceased	Cerebral seizure, non-obliterating thrombosis of the inferior vena cava, multiple fractures, tachypnea	Strabismus, renal dysplasia, respiratory distress, small choroid plexus bleed, low level of 25-hydroxy vitamin D	Asphyxia	Renal stone	Respiratory insufficiency, inflammatory condition, granulocyte hyperplasia, arthritis, stenosis of arteries, hemiplegic stroke, hypertension		Fetal distress			

UPD, uniparental disomy.

[a]Cutaneous abnormality: hemangioma, cutaneous capillary vascular malformation or pigmentation. Neurological abnormality: developmental and motor delay, hypotonia, convulsion or autism. Other abnormality: ear lobe anomaly, hypertelorism, abnormal facies, bell-shaped thorax, or others.

SNP array showed two normal copies of both regions (Fig. S2). Sanger sequencing revealed a single-base deletion in exon 10 of *SLC7A9*, which led to a previously reported frameshift mutation (c.1017delA, p.V340fsX21, RefSeq: NM_001126335) (10), whereas no mutation was found in *SLC3A1* (Fig. 2c). The father was a heterozygous carrier of the mutation showing moderately elevated cystine and lysine in his urine without urolithiasis, while the mother was homozygous for the wild-type allele (Fig. 2c). The patient seemed to be homozygous for the mutation because of the high mosaic ratio of GWpUPD (Fig. 2c,d). *In silico* prediction programs such as MutationTaster (http://www.mutationtaster.org/) and SIFT-indels (http://sift.bii.a-star.edu.sg/www/SIFT_indels2.html) predicted the *SLC7A9* mutation as 'DISEASE CAUSING' and 'DAMAGING', respectively. The mutation could not be found after a comprehensive database search covering dbSNP (http://www.ncbi.nlm.nih.gov/projects/SNP/), 1000 Genomes (http://www.1000genomes.org/), ClinVar (http://www.ncbi.nlm.nih.gov/clinvar/), the Human Genome Variation Database (http://www.genome.med.kyoto-u.ac.jp/SnpDB/index.html), and the Exome Variant Server (http://evs.gs. washington.edu/EVS/). Furthermore, we identified the *SLC7A9* mutation in DNA from the patient's urine (Fig. S3b).

On the basis of these findings we concluded that the patient was homozygous for the *SLC7A9* mutation in GWpUPD cells and heterozygous in biparental cells. Because a high ratio of mosaicism was found in the patient's urine (average mosaic rate: 76%) (Fig. S3a), we speculated that the high ratio of mosaicism also occurred in the patient's kidneys, which resulted in the observed cystinuria.

Discussion

In this study, we describe a patient concurrently afflicted with BWS and autosomal recessive cystinuria. Genetic analyses revealed that the patient, who possesses mosaic GWpUPD, is also homozygous for a *SLC7A9* mutation in GWpUPD cells, while her normal biparental cells are heterozygous. The mutation was inherited from the patient's father, who carried the mutation.

Approximately 20% of patients with BWS show mosaicism for pUPD11 (1). This segmental pUPD is considered to result from mitotic recombination at an early embryonic stage (11). A small number of reports exist that detail GWpUPD patients with BWS phenotypes (1). Fifteen patients with live-born mosaic GWpUPD, including our patient, have been described so far in 11 reports (Table 1) (4, 12–21). Although previous assumptions were of low GWpUPD incidence in pUPD11 patients, a recent report suggested that GWpUPD might actually be more frequent than expected because two GWpUPD patients were found out of 11 pUPD11 patients (22). All these patients showed only one paternal haplotype (isodisomy) and no evidence of any chromosomal crossing-over. This strongly suggests that a mechanism of mosaic GWpUPD involves normal fertilization followed by failure of maternal DNA replication and paternal genome endoreplication (12, 23, 24). These patients frequently show hyperinsulinemic hypoglycemia (12/15), often accompanied by nesidioblastosis, for which partial or near-total pancreatectomy may be required. The incidence of tumor development is much higher in GWpUPD patients (14/15) than in segmental pUPD11 (approximately 25%) (Table 1) (25). Several types of benign and malignant tumors develop metachronously and ectopically (12). Because segmental pUPD11 itself is a risk factor for tumor development, there may be additional factors in GWpUPD patients, such as as-yet poorly characterized imprinted regions and undiscovered recessive loci associated with cell growth or survival (12). The possibility of GWpUPD should be tested in patients with pUPD11 as a general, in particular to guard against their increased tumor risk.

Although other chromosomes, especially chromosomes 6, 14, 15, and 20, are also pUPD in GWpUPD patients, associated clinical features were seen less frequently with them, suggesting (epi)dominance of pUPD11 (Table 1). Yamazawa et al. suggested several determination factors for clinical features of mosaic GWpUPD, including the mosaic ratios in various tissues, dysregulation of imprinted domains, and unmasking of paternally inherited recessive mutations (4).

We found that our patient was homozygous for a one-base deletion mutation of *SLC7A9*, which is a causative gene for cystinuria. A GWpUPD patient has been previously reported to have renal calcium stones. However, the cause of the renal stones remains unknown (16). *SLC7A9* encodes $b^{+,0}$AT, which is a light subunit of the rBAT/$b^{0,+}$AT amino acid transporter expressed in the renal proximal tubule (5, 6). The mutation has been reported to decrease cystine transport activity drastically compared with wild-type rBAT/$b^{0,+}$AT *in vitro* (10). The loss of function of this transporter system leads to the formation of cystine stones in patients.

In conclusion, we report for the first time a patient concurrently affected by both BWS and autosomal recessive cystinuria. The genotype of this patient clearly indicates that a paternally inherited recessive mutation can cause a recessive disease in patients with mosaic GWpUPD. To understand the clinical conditions of patients with mosaic GWpUPD better, further investigation of dysregulation of imprinted domains and recessive mutations is necessary. To this end, whole exome sequencing would be useful in identifying paternally inherited recessive mutations.

Supporting Information

Additional supporting information may be found in the online version of this article at the publisher's web-site.

Acknowledgements

This study was supported, in part, by a Grant for Research on Intractable Diseases from the Ministry of Health, Labor, and Welfare; a Grant for Child Health and Development from the National Center for Child Health and Development; a Grant-in-Aid for Challenging Exploratory Research; and a Grant-in-Aid for Scientific Research (C) from the Japan Society for the Promotion of Science.

References

1. Choufani S, Shuman C, Weksberg R. Molecular findings in Beckwith-Wiedemann syndrome. Am J Med Genet C Semin Med Genet 2013: 163C: 131–140.
2. Soejima H, Higashimoto K. Epigenetic and genetic alterations of the imprinting disorder Beckwith-Wiedemann syndrome and related disorders. J Hum Genet 2013: 58: 402–409.
3. Romanelli V, Meneses HN, Fernández L et al. Beckwith-Wiedemann syndrome and uniparental disomy 11p: fine mapping of the recombination breakpoints and evaluation of several techniques. Eur J Hum Genet 2011: 19: 416–421.
4. Yamazawa K, Nakabayashi K, Matsuoka K et al. Androgenetic/biparental mosaicism in a girl with Beckwith-Wiedemann syndrome-like and upd(14)pat-like phenotypes. J Hum Genet 2011: 56: 91–93.
5. Barbosa M, Lopes A, Mota C et al. Clinical, biochemical and molecular characterization of cystinuria in a cohort of 12 patients. Clin Genet 2012: 81: 47–55.
6. Fotiadis D, Kanai Y, Palacín M. The SLC3 and SLC7 families of amino acid transporters. Mol Aspects Med 2013: 34: 139–158.
7. Weksberg R, Shuman C, Beckwith JB. Beckwith-Wiedemann syndrome. Eur J Hum Genet 2010: 18: 8–14.
8. Kubota A, Yonekura T, Usui N et al. Two cases of persistent hyperinsulinemic hypoglycemia that showed spontaneous regression and maturation of the Langerhans islets. J Pediatr Surg 2000: 35: 1661–1662.
9. Takama Y, Kubota A, Nakayama M et al. Fibroadenoma in Beckwith–Wiedemann syndrome with paternal uniparental disomy of chromosome 11p15.5. Pediatrics International 2014: in press.
10. Shigeta Y, Kanai Y, Chairoungdua A et al. A novel missense mutation of SLC7A9 frequent in Japanese cystinuria cases affecting the C-terminus of the transporter. Kidney Int 2006: 69: 1198–1206.
11. Yamazawa K, Nakabayashi K, Kagami M et al. Parthenogenetic chimaerism/mosaicism with a Silver-Russell syndrome-like phenotype. J Med Genet 2010: 47: 782–785.
12. Kalish JM, Conlin LK, Bhatti TR et al. Clinical features of three girls with mosaic genome-wide paternal uniparental isodisomy. Am J Med Genet A 2013: 161A: 1929–1939.
13. Johnson JP, Waterson J, Schwanke C et al. Genome-wide androgenetic mosaicism. Clin Genet 2014: 85: 282–285.
14. Inbar-Feigenberg M, Choufani S, Cytrynbaum C et al. Mosaicism for genome-wide paternal uniparental disomy with features of multiple imprinting disorders: diagnostic and management issues. Am J Med Genet A 2013: 161A: 13–20.
15. Gogiel M, Begemann M, Spengler S et al. Genome-wide paternal uniparental disomy mosaicism in a woman with Beckwith-Wiedemann syndrome and ovarian steroid cell tumour. Eur J Hum Genet 2013: 21: 788–791.
16. Romanelli V, Nevado J, Fraga M et al. Constitutional mosaic genome-wide uniparental disomy due to diploidisation: an unusual cancer-predisposing mechanism. J Med Genet 2011: 48: 212–216.
17. Wilson M, Peters G, Bennetts B et al. The clinical phenotype of mosaicism for genome-wide paternal uniparental disomy: two new reports. Am J Med Genet A 2008: 146A: 137–148.
18. Reed RC, Beischel L, Schoof J et al. Androgenetic/biparental mosaicism in an infant with hepatic mesenchymal hamartoma and placental mesenchymal dysplasia. Pediatr Dev Pathol 2008: 11: 377–383.
19. Giurgea I, Sanlaville D, Fournet JC et al. Congenital hyperinsulinism and mosaic abnormalities of the ploidy. J Med Genet 2006: 43: 248–254.
20. Bryke C, Garber A, Israel J. Evolution of a complex phenotype in a unique patient with a paternal uniparental disomy for every chromosome cell line and a normal biparental inheritance cell line. Toronto, Canada: The annual meeting of The American Society of Human Genetics, 2004: Program Number: 823.
21. Hoban PR, Heighway J, White GR et al. Genome-wide loss of maternal alleles in a nephrogenic rest and Wilms' tumour from a BWS patient. Hum Genet 1995: 95: 651–656.
22. Eggermann T, Heilsberg AK, Bens S et al. Additional molecular findings in 11p15-associated imprinting disorders: an urgent need for multi-locus testing. J Mol Med (Berl) 2014: 92: 769–777.
23. Kotzot D. Complex and segmental uniparental disomy updated. J Med Genet 2008: 45: 545–556.
24. Lapunzina P, Monk D. The consequences of uniparental disomy and copy number neutral loss-of-heterozygosity during human development and cancer. Biol Cell 2011: 103: 303–317.
25. Choufani S, Shuman C, Weksberg R. Beckwith-Wiedemann syndrome. Am J Med Genet C Semin Med Genet 2010: 154C: 343–354.

Pregnancy-associated microRNAs in plasma as potential molecular markers of ectopic pregnancy

Kiyonori Miura, M.D., Ph.D.,[a] Ai Higashijima, M.D., Ph.D.,[a] Hiroyuki Mishima, D.D.S., Ph.D.,[a] Shoko Miura, M.D., Ph.D.,[a] Michio Kitajima, M.D., Ph.D.,[a] Masanori Kaneuchi, M.D., Ph.D.,[a] Koh-ichiro Yoshiura, M.D., Ph.D.,[b] and Hideaki Masuzaki, M.D., Ph.D.[a]

[a] Department of Obstetrics and Gynecology, and [b] Department of Human Genetics, Nagasaki University Graduate School of Biomedical Sciences, Nagasaki, Japan

Objective: To investigate cell-free pregnancy-associated microRNAs as molecular markers for the diagnosis of ectopic pregnancy.
Design: Laboratory study using human plasma samples.
Setting: Research unit in a university hospital.
Patient(s): Plasma samples from 18 women with ectopic pregnancies (EP group), 12 women with spontaneous abortion (SA group), and 26 normal women with singleton pregnancies (NP group).
Intervention(s): Total RNAs containing small RNA molecules extracted from 1.2 mL of plasma.
Main Outcome Measure(s): Plasma concentrations of cell-free microRNAs measured by quantitative real-time reverse-transcriptase polymerase chain reaction.
Result(s): Plasma concentrations of cell-free pregnancy-associated microRNAs (miR-323-3p, miR-515-3p, miR-517a, miR-517c, and miR-518b) and serum concentration of human chorionic gonadotropin (hCG) were confirmed to have statistically significantly different plasma or serum concentrations in women with EP, SA, or NP. There was no statistically significant difference in the plasma concentrations of cell-free miR-21 between the three groups. By correlation coefficient analysis, no relationship was detected between serum hCG levels and plasma cell-free miR-517c, miR-515-3p, miR-517a, miR-518b, miR-323-3p, or miR-21 levels. Plasma concentrations of cell-free miR-517a could distinguish EP/SA from NP, yielding an area under the curve of 0.9654 (95% confidence interval, 0.9172–1.0). Plasma concentrations of cell-free miR-323-3p could distinguish EP from SA, yielding an area under the curve of 0.7454 (95% confidence interval, 0.5558–0.9349).
Conclusion(s): Cell-free pregnancy-associated microRNAs have potential as molecular markers of ectopic pregnancy. (Fertil Steril® 2015;103:1202–8. ©2015 by American Society for Reproductive Medicine.)
Key Words: Biomarker, ectopic pregnancy, pregnancy-associated microRNA, plasma

Discuss: You can discuss this article with its authors and with other ASRM members at http://fertstertforum.com/miurak-pregnancy-associated-micrornas-ectopic-pregnancy/

Use your smartphone to scan this QR code and connect to the discussion forum for this article now.*

* Download a free QR code scanner by searching for "QR scanner" in your smartphone's app store or app marketplace.

Ectopic pregnancy (EP), in which a conceptus implants outside the endometrial cavity, occurs in approximately 1% to 2% of pregnant women (1, 2). Currently, serum human chorionic gonadotropin (hCG) and/or progesterone are used as biomarkers for early detection of ectopic pregnancy. When ultrasonography can identify the gestational sac outside the endometrial cavity, ectopic pregnancies can be easily diagnosed and medical or surgical therapy can be promptly provided. However, when ultrasonography is not definitive, serial biochemical assessment using serum hCG and/or progesterone is necessary (3, 4). With the use of serial serum hCG measurements, patients are at risk of tubal rupture during the delay before the next hCG measurement. Moreover, the use of serum hCG and/or progesterone to identify ectopic pregnancy is limited by high false-positive and false-negative rates (3, 4). Therefore, additional markers to diagnose ectopic pregnancies during early pregnancy are necessary.

Received August 29, 2014; revised January 25, 2015; accepted January 28, 2015; published online March 13, 2015.
K.M. has nothing to disclose. A.H. has nothing to disclose. H.Mi. has nothing to disclose. S.M. has nothing to disclose. M.Ki. has nothing to disclose. M.Ka. has nothing to disclose. K.-I.Y. has nothing to disclose. H.Ma. has nothing to disclose.
Supported by JSPS KAKENHI, grant numbers 26462495, 24791712, and 25462563 (to K. Miura, S. Miura, and H. Masuzaki, respectively).
Reprint requests: Kiyonori Miura, M.D., Ph.D., Department of Obstetrics and Gynecology, Nagasaki University Graduate School of Biomedical Sciences, 1–7–1 Sakamoto, Nagasaki 852–8501, Japan (E-mail: kiyonori@nagasaki-u.ac.jp).

Fertility and Sterility® Vol. 103, No. 5, May 2015 0015-0282/$36.00

http://dx.doi.org/10.1016/j.fertnstert.2015.01.041

Recently, pregnancy-associated microRNAs (miRNAs) circulating in maternal plasma were reported (5, 6), and we also identified pregnancy-associated miRNAs (miR-515-3p, miR-517a, miR-517c, miR-518b, miR-526b, and miR-323-3p) in the plasma of pregnant women (7). To date, only one study has reported the potential usefulness of circulating pregnancy-associated miRNAs as biomarkers of ectopic pregnancy (4). In this study, plasma concentrations of miR-517a, miR-519d, and miR-525-3p were significantly lower in EP or spontaneous abortion (SA) than in normal pregnancies (NP), while plasma concentrations of miR-323-3p were significantly higher in EP than in NP or SA (4). However, this observation has not been independently confirmed, and the diagnostic value of cell-free pregnancy-associated miRNAs for EP remains unknown.

Herein, to obtain information of pregnancy-associated miRNAs as potential molecular markers for the diagnosis of EP during early pregnancy, we investigated circulating levels of pregnancy-associated miRNA in plasma from women with EP, SA, and NP in an independent population of a previous study (4). Subsequently, the diagnostic value of circulating pregnancy-associated miRNAs levels in plasma for the identification of EP was analyzed.

MATERIALS AND METHODS

Sample Collection

All pregnant women recruited for this study attended Nagasaki University Hospital. All samples were obtained after receiving informed written consent, and the institutional review board for ethical, legal and social issues of Nagasaki University approved the study protocol.

All the pregnant women in this study visited Nagasaki University Hospital exhibiting symptoms of vaginal bleeding and abdominal pain early in the first trimester. We obtained blood samples (7 mL) from 18 pregnant women with ectopic pregnancies (the EP group), 12 pregnant women with spontaneous abortion (the SA group), and 26 normal singleton-pregnant women (the NP group) during the first trimester (ranging from 6 to 10 weeks of gestation). Among the three groups, there were no statistically significant differences in maternal age or gestational age at blood sampling (Table 1).

When the urine hCG test was positive (>50 mIU/mL) but an intrauterine pregnancy was not detected by ultrasound, the possibility of EP, SA, or NP was suspected. When the serial hCG measurements later showed an increasing hCG level but an intrauterine pregnancy was still undetected, diagnostic confirmation and treatment of EP were performed by laparoscopy. All diagnoses of ectopic pregnancies were confirmed clinically by ultrasound, serial hCG measurements, and histopathology. When the serial monitoring of serum hCG ultimately resulted in a negative hCG level and no intrauterine pregnancy was detected, the pregnancy was diagnosed as SA.

To confirm the location of the pregnancy in the SA group or to eliminate the possibility of simultaneous intrauterine and ectopic pregnancies, intrauterine curettage was performed in all cases of SA (n = 12) and EP (n = 18). The existence of villus tissue in the uterus was confirmed in 10

TABLE 1

Patient age, gestational age, serum concentrations of hCG, and plasma concentrations of cell-free microRNAs in women with spontaneous abortion, ectopic pregnancy, or normal pregnancy.

Characteristic	SA group (n = 12)	EP group (n = 18)	NP group (n = 26)	*P* value			
				Kruskal-Wallis test	EP vs. SA	EP vs. NP	SA vs. NP
Maternal age (y)	32.18 (2.86)	31.78 (5.96)	32.42 (2.58)	NS	NS[a]	NS[a]	NS[a]
GA (wk)	7.52 (1.06)	7.89 (1.23)	8.31 (1.31)	NS	NS[a]	NS[a]	NS[a]
hCG (mIU/mL)	2,943.5 (474.0–17,000.0)	5,032.0 (306.6–195,510.0)	75,044.0 (35,461.0–220,510.0)	< .001	NS[b]	< .001[b]	< .001[b]
miR-323-3p (MoM)	0.6528 (0.51–2.60)	1.5499 (0.18–133.07)	1.00 (0.24–9.28)	.044	NS[b]	NS[b]	NS[b]
miR-21 (MoM)	0.8233 (0.30–1.74)	0.9692 (0.34–2.83)	1.00 (0.64–1.79)	NS	NS[b]	NS[b]	NS[b]
miR-517c (MoM)	0.1823 (0.00–0.86)	0.2672 (0.00–4.14)	1.00 (0.45–5.45)	< .001	NS[b]	.021[b]	.003[b]
miR-515-3p (MoM)	0.2208 (0.00–0.34)	0.0432 (0.00–0.83)	1.00 (0.08–3.62)	< .001	NS[b]	< .001[b]	< .001[b]
miR-517a (MoM)	0.0693 (0.02–1.45)	0.0459 (0.00–0.76)	1.00 (0.41–5.16)	< .001	NS[b]	< .001[b]	< .001[b]
miR-518b (MoM)	0.5898 (0.18–1.32)	0.46 (0.04–3.27)	1.00 (0.04–71.39)	.009	NS[b]	NS[b]	NS[b]

Note: Patient age and gestational age at blood sampling in the spontaneous abortion (SA), ectopic pregnancy (EP), and normal pregnancy (NP) groups are indicated as mean and standard deviation. Serum hCG levels and plasma cell-free microRNA (miRNA) levels are indicated as median (minimum–maximum). Significant differences between groups were analyzed by Student's *t* test, Kruskal-Wallis test, or Bonferroni correction for post hoc analysis of multiple comparisons. $P < .05$ was considered statistically significant, except for the multiple comparisons of clinical data where a Bonferroni correction was applied. NS = not statistically significant.

[a] Student's *t* test.

[b] Bonferroni correction.

Miura. Ectopic pregnancy-associated miRNAs. Fertil Steril 2015.

cases of SA but not in two cases of SA or any of the 18 cases of EP. Therefore, a pregnancy of unknown location was present in two cases of SA. The gestational age of the EP and SA groups was calculated from the date of the woman's last menstrual period.

When the serial hCG measurements showed an increasing hCG level and an intrauterine pregnancy was detected later, the pregnancy was diagnosed as a normal pregnancy. For all normal pregnancies, an intrauterine gestational sac containing a yolk sac was identified by transvaginal ultrasound. Gestational age in the NP group was confirmed by ultrasonographic examination, and the crown-rump length of the fetus at 8 to 10 weeks' gestation was measured.

Blood samples were collected in tubes containing ethylenediaminetetraacetic acid (EDTA). As cell-free RNA is known to be stable in plasma samples (8, 9), cell-free plasma samples were prepared from maternal blood using a double centrifugation method, as described previously elsewhere (5, 7, 10). Briefly, after the first centrifugation at 3,000 × *g* for 10 minutes, the supernatant was stored immediately in a refrigerator at −80°C. Within 6 months, the plasma samples were centrifuged at 16,000 × *g* for 10 minutes, and 1.2 mL of their supernatants (double-centrifuged plasma samples) were used as the plasma samples for the extraction of cell-free RNA. Cell-free RNA containing small RNA molecules (ranging from 40 to 60 ng/μL) was extracted from 1.2 mL of maternal plasma using the *mir*Vana miRNA Isolation Kit (Ambion) according to the manufacturer's instructions. The concentrations of cell-free RNA were measured by Nanodrop, and A260/A230 showed >1.8 in all extracted RNA samples.

Real-time Quantitative Reverse Transcriptase Polymerase Chain Reaction Analysis of miRNAs

Pregnancy-associated placenta-specific miRNAs (miR-515-3p, miR-517a, miR-517c, and miR-518b), pregnancy-associated but not placenta-specific miRNA (miR-323-3p), miR-21 (expressed in maternal, fetal, and placenta tissues), and U6 snRNA (mature miRNA internal control) were analyzed in this study (5, 7, 11, 12). All specific primers and TaqMan probes were purchased from TaqMan MicroRNA Assays (Life Technologies).

The real-time quantitative reverse transcriptase polymerase chain reaction (qRT-PCR) of the miRNAs in plasma samples was performed as described previously elsewhere (5, 7, 13, 14). Initially, 2.5 ng of RNA samples were used in the reverse transcriptase step. Subsequently, for real-time quantitative PCR of miRNAs, we prepared a calibration curve by 10-fold serial dilution of single-stranded cDNA oligonucleotides corresponding to each miRNA sequence from 1.0×10^2 to 1.0×10^8 copies/mL for each miRNA assay. Each sample and each calibration dilution were analyzed in triplicate. Each assay was capable of detecting down to 300 RNA copies/mL (7, 13, 14). Every batch of amplifications included three water blanks as negative controls for each of the reverse transcription and PCR steps.

All data were collected and analyzed using a LightCycler 480 Real-Time PCR System (Roche). It was recommended that the quantitative mRNA measurements in plasma samples be expressed as an absolute concentration (15). Therefore, we considered that the quantitative miRNA measurements were potentially the same as the quantitative mRNA measurements in plasma. Hence, an absolute real-time qRT-PCR analysis was performed. As an internal control during quantitative PCR, we used the concentration of U6 snRNA in each sample. In each sample, the plasma concentrations of target miRNAs were adjusted by the plasma concentrations of U6 snRNA. By using QIAgility (Quiagen), a compact benchtop instrument that enables rapid, high-precision PCR setup, we could place 66 samples in triplicate on a plate with the standard curves and negative controls. The experiments were run on the same 384-well plate. The intra-assay coefficients of variation, which were the ratios of the standard deviation to the mean for the probes in the absolute qRT-PCR, were 8.1% for miR-518b, 7.2% for miR-517a, 6.1% for miR-515-3p, 5.6% for 517a, 6.7% for miR-323-3p, 6.9% for miR-21, and 6.2% for U6 snRNA.

Statistical Analysis

The patients' backgrounds for the SA, EP and NP groups were compared using Student's *t* test for continuous variables. The plasma concentrations of cell-free miRNAs in three groups were converted into multiples of the median value in the NP group and were adjusted for gestational age. The differences among the three groups were evaluated using the Kruskal-Wallis test. The differences between two groups were evaluated using Bonferroni correction for post hoc analysis of multiple comparisons. Statistical analyses were performed with SPSS version 19 (IBM Corporation). Pearson product-moment correlation coefficients between plasma concentrations of cell-free miRNAs and serum hCG levels were analyzed with SPSS version 19 (IBM Corporation). To eliminate spurious correlations between the circulating levels of cell-free miRNAs and the serum hCG levels, a partial correction coefficient analysis was performed. $P<.05$ was considered statistically significant, except for the multiple comparisons of clinical data where a Bonferroni correction was applied. To determine the ability of miRNAs to classify EP, SA, and NP, we plotted receiver operating characteristic (ROC) curves with the R package pROC (http://expasy.org/tools/pROC/) (16). Statistical analyses were performed using R software (R Core Team).

RESULTS

Circulating Levels of Serum hCG and Plasma Cell-free miRNAs in the Spontaneous Abortion, Ectopic Pregnancy and Normal Pregnancy Groups

Human chorionic gonadotropin (hCG) was confirmed to have statistically significantly different serum concentrations in women with EP, SA, or NP (Kruskal-Wallis test; see Table 1; and Supplemental Fig. 1, available online). Also, cell-free pregnancy-associated miRNAs (miR-323-3p, miR-515-3p, miR-517a, miR-517c, and miR-518b) were confirmed to have statistically significantly different plasma concentrations in women with EP, SA, or NP (Kruskal-Wallis test; see Table 1, Supplemental Fig. 1). However, there was no

statistically significant difference in the plasma cell-free miR-21 levels among the three groups (Kruskal-Wallis test; see Table 1, Supplemental Fig. 1).

The serum concentrations of hCG in the EP or SA groups were statistically significantly lower than in NP group ($P<.001$; see Table 1). There was no significantly significant difference in serum hCG levels between the EP and SA groups (see Table 1). The plasma concentrations of cell-free pregnancy-associated placenta-specific miRNAs (miR-515-3p, miR-517a, and miR-517c) in the EP and SA groups were statistically significantly lower than in the NP group ($P<.001$ for all three miRNAs; see Table 1, Supplemental Fig. 1). There were no statistically significant differences in the plasma cell-free miR-515-3p, miR-517a, miR-517c, and miR-518b levels between the EP and SA groups (see Table 1, Supplemental Fig. 1). There was no statistically significant difference of plasma cell-free pregnancy-associated but not placenta-specific microRNA (miR-323-3p) levels between the EP and SA groups, between the EP and NP groups, or between the SA and NP groups (see Table 1).

Association between Serum Concentration of hCG and Plasma Concentration of Cell-free Pregnancy-associated miRNA in Pregnant Women

Pearson product-moment correlation coefficient analysis or partial correction coefficient analysis showed no association between the serum concentration of hCG and the plasma concentration of cell-free miRNAs (Table 2).

Diagnostic Value of Pregnancy-associated miRNA Concentration in Plasma

We constructed ROC curves for discriminating EP/SA from NP based on the plasma concentration of cell-free pregnancy-associated miRNA and the serum concentration of hCG. Our analysis of the ROCs revealed high area under the curve (AUC) values for each pregnancy-associated miRNA in plasma and hCG in serum (Fig. 1): miR-518b, miR-517a, miR-515-3p, miR-517c, miR-323-3p, and hCG yielded AUCs of 0.7372 (95% confidence interval [CI], 0.6046–0.8698), 0.9654 (95% CI, 0.9172–1.0000), 0.9141 (95% CI, 0.8405–0.9877), 0.9077 (95% CI, 0.8192–0.9962), 0.5821 (95% CI, 0.4279–0.7362), and 0.9654 (95% CI, 0.9046–1.0000), respectively (see Fig. 1).

We constructed ROC curves for discriminating EP from SA based on the plasma concentration of cell-free pregnancy-associated miRNA and the serum concentration of hCG. Our analysis of the ROCs revealed high AUC values for each pregnancy-associated miRNA in plasma and hCG in serum (Fig. 2): miR-518b, miR-517a, miR-515-3p, miR-517c, miR-323-3p, and hCG yielded AUCs of 0.5602 (95% CI, 0.3479–0.7725), 0.5278 (95% CI, 0.3118–0.7438), 0.6713 (95% CI, 0.4710–0.8716), 0.5972 (95% CI, 0.3873–0.8072), 0.7454 (95% CI, 0.5558–0.9349), and 0.6019 (95% CI, 0.3902–0.8135), respectively (see Fig. 2).

DISCUSSION

In this study, we confirmed the clinical significance of cell-free pregnancy-associated miRNAs in plasma samples from EP in an independent population of a previous study (4). First, the plasma concentrations of cell-free pregnancy-associated placenta-specific microRNA (miR-515-3p, miR-517a, miR-517c, and miR-518b) were confirmed to be statistically significantly different in women with EP, SA, or NP; therefore, we could confirm the previously reported data that pregnancy-associated placenta-specific microRNAs were candidate markers and statistically significant different among the three groups (4). We showed decreased levels of cell-free pregnancy-associated placenta-specific miRNAs (miR-517a, miR-515-3p, and miR-517c) in plasma

TABLE 2

Summary of correlation coefficient analysis between serum concentrations of hCG and plasma concentration of cell-free pregnancy-associated microRNAs in pregnant women.

			Serum hCG level	
Plasma miRNA level	Expression pattern	Statistical analysis	*r* value	*P* value
miR-515-3p	Placenta-specific expression	Pearson product-moment correlation coefficient	0.457	<.001
		Partial correction coefficient[a]	0.258	.060
miR-517a	Placenta-specific expression	Pearson product-moment correlation coefficient	0.452	<.001
		Partial correction coefficient[b]	0.237	.084
miR-517c	Placenta-specific expression	Pearson product-moment correlation coefficient	0.332	.013
		Partial correction coefficient[c]	−0.080	.565
miR-518b	Placenta-specific expression	Pearson product-moment correlation coefficient	0.110	.418
miR-323-3p	Embryonic and placental expression	Pearson product-moment correlation coefficient	−0.111	.414
		Partial correction coefficient[d]	−0.179	.192
miR-21	Expressed in multiple tissues including maternal, fetal, and placental tissues	Pearson product-moment correlation coefficient	0.019	.891
		Partial correction coefficient[e]	−0.089	.526

Note: $P<.05$ was considered statistically significant. To eliminate spurious correlation between serum human chorionic gonadotropin (hCG) concentrations and plasma cell-free microRNAs (miRNAs), a partial correction coefficient analysis was performed.

[a] Data from miR-517a and miR-517c as control variable.
[b] Data from miR-21, miR-517c, and miR-515-3p as control variable.
[c] Data from miR-21, miR-515-3p, and miR-517a as control variable.
[d] Data from miR-21 as control variable.
[e] Data from miR-323-3p, miR-517c, and miR-517a as control variable.

Miura. Ectopic pregnancy-associated miRNAs. Fertil Steril 2015.